VALIDATION OF MERIS-DERIVED TURBIDITY AND PAR ATTENUATION USING AUTONOMOUS BUOY DATA

Quinten Vanhellemont [(1)], Naomi Greenwood [(2)], Kevin Ruddick [(1)]

[(1)] Royal Belgian Institute of Natural Sciences, Operational Directorate Natural Environment, Gulledelle 100, 1200 Brussels, Belgium, Email: quinten.vanhellemont@mumm.ac.be
[(2)] Centre for Environment, Fisheries and Aquaculture Science, Lowestoft, Suffolk, NR33 0HT, UK

ABSTRACT

Ocean colour remote sensing is becoming well-established for the monitoring of coastal waters. However, validation of satellite-derived products remains problematic, as matchups of in situ data and cloud-free satellite data are costly and difficult to obtain with ship-based measurements. We present a validation of several MERIS algorithms for turbidity (T) and attenuation of photosynthetically active radiation (K_{PAR}), using measurements from three autonomous buoys in coastal waters, two in the North Sea, and one in the Irish sea. In situ data were combined with marine reflectance spectra and level 2 products from multiple processing versions. The merged dataset contains several hundreds of matchups and allows for flexible testing of retrieval algorithms for T and K_{PAR}. Autonomous systems prove to be powerful tools for validating satellite data in dynamic coastal waters, where changes occur quickly both in space and time.

1. INTRODUCTION

The collection of ship-borne data to validate remote sensing products is expensive, and gives a low number of matchups per year, even with dedicated campaigns. Optical instruments on autonomous platforms can provide many more matchups, typically one per cloud-free image. For moderate resolution ocean colour sensors such as ENVISAT/MERIS (2002-2012) this means at least one matchup per cloud-free day at mid-latitudes, giving tens of matchups per year and hundreds over the lifetime of the satellite. SmartBuoys [1] are an example of such autonomous buoys, and have been deployed by CEFAS for many years, some for over a decade. These buoys record several parameters multiple times per hour, with only short disruptions between deployments. Even though the SmartBuoys were not designed for satellite validation, they have been successfully used for that purpose [2] [3] [4]. Here we have put together a dataset of matching satellite and in situ data, for similar validation or algorithm testing.

2. METHODS

2.1 In situ data

The buoys used in this study are located in UK coastal waters (Figure 1), at Warp Anchorage (WARP, approx. 51.53°N, 1.03°E), West Gabbard (WGAB, approx. 51.98°N, 2.08°E) and Liverpool Bay (LIVB, approx. 53.53°N, 3.36°W). SmartBuoys collect measurements of salinity and temperature using various sensors, fluorescence with a Seapoint Fluorometer, and turbidity (T) with a Seapoint Turbidity Meter that emits a light at 880 nm and has a wide acceptance angle of 15-150°. Downwelling photosynthetically active radiation (PAR) is measured with a LI-192 Underwater Quantum Sensor in the range 400-700 nm with a flat cosine collector, at 1 and 2 m depth at LIVB and at 0^+, 1, and 2 m depth at WARP and WGAB. The mean average from burst measurements of several minutes (usually 10) at 1 Hz is recorded every fifteen, twenty or thirty minutes (depending on deployment). After retrieval the data are post processed and quality controlled (details omitted). The PAR measurements can be used to estimate the diffuse attenuation coefficient of PAR (K_{PAR}) at 1.5 m depth:

$$K_{PAR}(1.5m) = \ln\left(\frac{PAR(1m)}{PAR(2m)}\right) * 1m^{-1} \qquad 1$$

The in situ K_{PAR} data is quality controlled using the 0^+ m PAR measurements with rejection of points where K_{PAR} at 1.5 m differs more than 50% from K_{PAR} at 0.5 m. Data from LIVB is excluded as it lacks a 0^+ m measurement.

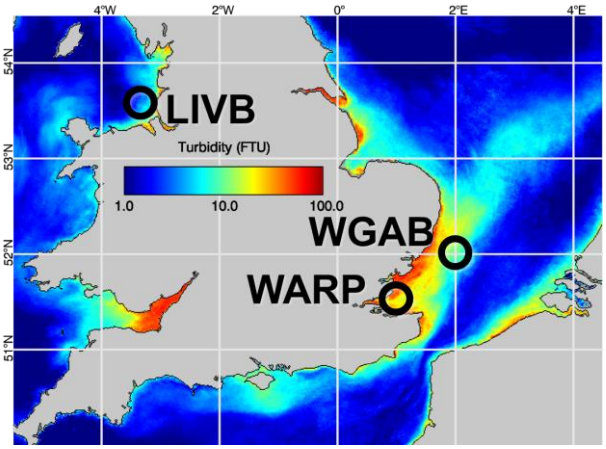

Figure 1 Location of the buoys on a composite of 2010 MERIS R3 T-Nechad (681 nm) turbidity, see further.

Submitted for the Proceedings of the 2013 European Space Agency Living Planet Symposium, held in Edinburgh 8-13 September 2013, ESA Special Publication SP-722.

2.2 Satellite data

Level 2 data from three MERIS processing versions were used: MEGS7.4, the 'second reprocessing' [5], MEGS8.0, the 'third reprocessing' [6] and the SeaDAS R2012.1 processing [7], hereafter referred to as M7, M8 and SD. For each scene covering a given buoy, marine reflectances and products were extracted from a 5x5 pixel box (kernel) over the pixel closest to the buoy's deployment location. Data were filtered using level 2 quality flags (Table 1). The buoy pixel value and the number of valid pixels, the mean average, median and standard deviation in the kernel were stored. The satellite data is then matched with the closest available in situ data within one hour (usually less).

MEGS	l2_flags (CLOUD, HIGH_GLINT) + appropriate PCD
SeaDAS	l2_flags (CLOUD, HISUNGLINT, LOWLW, MAXAERITER, HILT, STLIGHT) + Rrs (413, 443, 490) < 0, aot_865 < 0

Table 1: Quality screening for MEGS and SeaDAS.

2.3 Remote sensing algorithms

Satellite products were calculated from the best quality matchups, i.e. with 25/25 valid pixels in the surrounding kernel. Matching satellite and in situ data were compared using an ordinary least squares log-log regression. The 50, 5 and 95 percentiles of prediction errors (PE), the root mean square error (RMSE) and the coefficient of variation (CV) of the RMSE (dividing the RMSE by the mean of the observations) are given.

Two turbidity algorithms are compared over the three processing versions, T-Nechad [8] and T-Ouillion [9]. T-Nechad is a single band semi-empirical turbidity algorithm of the form:

$$T = A\frac{\rho_w}{C - \rho_w} + B \qquad 2$$

The algorithm was recalibrated with 68 in situ measurements, details in Section 5.6.1 of [10]. A, C and B coefficients for the MERIS bands are given in Table 2. The B offsets are small and represent measurement and model errors, and are not applied. The T-Ouillon algorithm was developed for tropical waters, but the relationship between ρ_w and turbidity (particulate side-scattering at 860 nm) is not expected to vary much between water types. The proposed global algorithm is a switching algorithm; first a single band (681 nm) 'turbid' water algorithm is calculated, using either the power law algorithm:

$$T_{power} = C_1 * Rrs\ 681^3 + C_2 * Rrs\ 681^2 + C_3 * Rrs\ 681 + C_4 \qquad 3$$

with coefficients C_1=-6204217, C_2=179652, C_3=36.49 and C_4=0.452, or the polynomial algorithm, which the authors suggest for the more turbid waters:

$$T_{poly} = 3183 * Rrs\ 681^{1.254} \qquad 4$$

Where the 'turbid' algorithm gives < 1 FTU the results are replaced with the three band 'clear' algorithm:

$$T_{clear} = 90.647 * \left(\frac{Rrs\ 620 * Rrs\ 681}{Rrs\ 412}\right)^{0.594} \qquad 5$$

Two K_{PAR} algorithms for MERIS were compared. The first, K_{PAR}-Devlin, uses the empirical relationship found in UK coastal waters [11]:

$$K_{PAR} = 0.325\ m^{-1} + 0.066\ m^2 g^{-1} * SPM \qquad 6$$

With SPM (suspended particulate matter, gm^{-3}) calculated with a semi-empirical single band algorithm using the 681 nm band [12]. This algorithm has the same form as Equation 2 but is calibrated with SPM measurements (Table 3), details in Section 5.6.1 of [10].

Wavelength (nm)	A_T (FNU)	C_T (-)	B_T (FNU)
560	89.0	0.1485	-0.28
620	188.2	0.1533	-0.10
665	296.8	0.1728	-0.22
681	320.8	0.1792	-0.33
708	451.8	0.1887	-0.22
753	1283.0	0.1997	-0.24
865	1264.7	0.2007	-0.25

Table 2: T-Nechad coefficients for MERIS bands.

Wavelength (nm)	A_T (g/m^3)	C_T (-)	B_T (g/m^3)
560	87.6	0.1189	-0.25
620	182.3	0.1533	-0.04
665	285.6	0.1728	-0.14
681	306.5	0.1792	-0.23
708	435.5	0.1887	-0.14
753	1270.3	0.1997	-0.22
865	1248.0	0.2007	-0.22

Table 3: SPM-Nechad coefficients for MERIS bands.

The second K_{PAR} algorithm is the semi-analytical algorithm from [13]. The inherent optical properties, a(490) and b_b(490) required for this algorithm were derived using the Quasi Analytical Algorithm [14] (QAA). Since these are turbid coastal stations, the 665 nm band was used as reference wavelength in the QAA.

3. RESULTS AND DISCUSSION

3.1 T-Nechad

In general good correlation coefficients are found for T-

Nechad, R^2 = 80–85%, with median prediction errors (PE50) of 17–25% (Figure 2). In these waters, the 665 nm and 681 nm bands perform best, perhaps with a slightly better performance for the 681 nm band. For these two bands the R^2 is lowest for M7 and highest for SD. There is little difference in PE50 between the processing versions. An underestimation of low T points is found that increases with wavelength. In SD there is a flattening towards a detection limit of ~40 FTU (WARP). These points are flagged in M7 and M8.

The RMSE increases from M7 to M8 to SD, as does the number of high T points. The RMSE of SD is also higher due to the detection limit mentioned above, as these high T points are (sometimes significantly) underestimated. When looking at the CV of the RMSE, all three processing versions perform similarly. M7 still has a lower RMSE(CV) than M8 and SD. Because of processor differences, the number of compared points in each plot is different; M7 has a lower number of matchups probably due to a more restrictive PCD_1_13 flag. When restricting the comparison to points present in all three datasets (n=178), SD performs best as the badly performing high T points are excluded.

3.2 T-Ouillon

For the single band 'turbid' algorithms, T_{power} and T_{poly} good correlation coefficients are found (Figure 3), R^2 = 75–83%, PE50 are higher than with T-Nechad: 27–31%. Regarding correlation and error statistics, the 'clear' algorithm performs similarly to the 'turbid' algorithms, albeit with a slope significantly lower than 1. T_{poly} reaches a maximum at T ~23.5 FTU, corresponding to Rrs681 of ~0.02 sr^{-1}. This saturation is clearly found at the WARP station, where Rrs681 is regularly greater than 0.02 sr^{-1}, i.e. in slightly under 23% of the MERIS images with 25/25 valid pixels in the kernel around the station. Of the 'turbid' retrievals 35–54 points (~10%) are <1 FTU, and are thus replaced with the 'clear' algorithm in the merged product. This results in a significant reduction of scatter in the low T points, albeit with an ambiguous impact on correlation statistics and errors: some improve, some do not.

3.3 Scatter in turbidity plots

There is still considerable scatter in the comparisons between satellite and in situ data that is difficult to attribute to a single source. A large contribution to the scatter is probably caused by the discrepancy in sampling volumes between the in situ sensor - a few cm^3 at one metre depth - and the satellite - integrated over 1 km^2 surface and the optical depth. In dynamic tidal systems like these, the characteristics of the measured volume can change on relatively short time scales. Therefore an additional more stringent quality check is applied: only matchups are included where:

1) the coefficient of variation in the in situ burst measurement is <10%, excluding waters with patchy suspended sediment concentrations, and
2) the time difference between in situ and satellite data is <10 minutes, excluding rapid temporal variations.

This additional filtering shows a quite large reduction in scatter, coupled with an improvement on R^2, now ranging between 84–90% and 73–88% respectively for T-Nechad (Figure 4) and T-Ouillon (not shown). Overall, PE50 are lower by a few percent. It is noted that the criterion on the in situ data results in the strongest reduction of the scatter (not shown separately), likely because the integrated value over the satellite pixel changes much less rapidly than the small volume of water seen by the buoy sensor.

3.4 K_{PAR}

It is clearly illustrated by the K_{PAR}-Devlin algorithm that in these waters K_{PAR} is dominated by SPM (Figure 5). Correlation (R^2 respectively 78–87% and 73–85%) and error statistics (PE50 13–19% and 18–24%) show a better fit for K_{PAR}-Lee than for K_{PAR}-Devlin. The slope of K_{PAR}-Lee is however quite different from 1, mainly because of the underestimation of the high K_{PAR} points (between 1-2 m^{-1}), where the QAA should be pushed to a longer reference wavelength (Lee, pers. comm.). Whereas SD showed underestimation for high T points, this discrepancy is not visible in the K_{PAR} comparison.

In some points however, K_{PAR}-Devlin underestimated with respect to the SmartBuoys. These points correspond to a fluorescence peak in the in situ data in early spring (April), very likely an algal bloom. In fact, most points below the 1:1 line have a relatively high in situ fluorescence. This is a weakness in the K_{PAR}-Devlin formulation, which ignores the impact of algae on the K_{PAR}, especially obvious in situations with relatively low SPM and high algal biomass. The same points are found near the centre of the point cloud in the K_{PAR}-Lee formulation. After filtering out data with in situ fluorescence > 2 (not shown here) the R^2 of K_{PAR}-Devlin is improved to 83–91%, with PE50 of 16–19%. For K_{PAR}-Lee, this filter also improves R^2 to 81–90%, median errors change little.

4. CONCLUSIONS

In the present study the performance of the three MERIS processors was quite comparable. The SD processor does consequently show higher R^2 values, with most of the time lower median errors, than the M7 and M8 processing. SD and M8 give more matchups than M7, largely because of the restrictive PCD_1_13 flag in M7. All processors seem limited for the most turbid waters, where M7 and M8 do not provide data and SD underestimates.

From the turbidity algorithms presented here, T-Nechad at 681 nm seemed to perform best; however, the differences between algorithms were small. T-Ouillon shows the advantages of a switching algorithm: the scatter in the low turbidity points significantly reduces by switching to a 'clear' algorithm. In coastal waters, K_{PAR} is often dominated by sediments and then the simple empirical relationship K_{PAR}-Devlin performs well, and has a slope close to 1. K_{PAR}-Lee shows better statistical performance, but its slope is quite different from 1. Both algorithms benefit from removing points with high in situ fluorescence.

It is shown that in highly variable systems even with moderately strict criteria, i.e. matchups within 60 minutes, considerable scatter remains for satellite-in situ turbidity comparisons. For closely timed (<10 minutes) matchups with low in situ variability, the scatter, but also the number of points, is strongly reduced. The importance of quasi-concurrent observations was also illustrated with time-shifted matchups by [4]. The advantage of continuously measuring autonomous systems for satellite validation, especially in highly dynamic coastal waters, where closely timed matchups are essential, is clear. These systems can typically provide a matchup per cloud-free pixel.

ACKNOWLEDGMENTS

This study was partially supported by 1) the STEREO programme of the Belgian Federal Science Policy Office (BELSPO) in the framework of the JELLYFOR-BE project (SR/37/135) and 2) by the BELSPO - PRODEX office BEL-AERONET project. SmartBuoy data were collected under Defra contract SLA25. ESA and NASA are thanked for the satellite data.

5. REFERENCES

[1] D. Mills, R. Laane, J. Rees, M. Rutgers van der Loeff, J. Suylen, D. Pearce, D. Sivyer, C. Heins, K. Platt and M. Rawlinson, "SmartBuoy: A marine environmental monitoring buoy with a difference.," in *Proc. Third International Conference on EuroGOOS.*, 2003.

[2] G. Neukermans, K. G. Ruddick and N. Greenwood, "Diurnal variability of turbidity and light attenuation in the southern North Sea from the SEVIRI geostationary sensor," *Remote Sensing of Environment*, vol. 124, pp. 564-580, 2012.

[3] B. Nechad, A. Alvera-Azcarate, K. Ruddick and N. Greenwood, "Reconstruction of MODIS total suspended matter time series maps by DINEOF and validation with autonomous platform data.," *Ocean Dynamics*, vol. 61, no. 8, p. 1205–1214, 2011.

[4] Q. Vanhellemont, G. Neukermans and K. Ruddick, "Synergy between polar-orbiting and geostationary sensors: Remote sensing of the ocean at high spatial and high temporal resolution.," *Remote Sensing of Environment*, in press.

[5] MERIS Quality Working Group, "MERIS 2nd reprocessing: Changes Description. Version 2." http://earth.eo.esa.int/pcs/envisat/meris/documentation/MERISRRsecondreprocessing-V2.pdf, 2005.

[6] MERIS Quality Working Group, "MERIS 3rd data reprocessing. Software and ADF updates" http://http://earth.eo.esa.int/pcs/envisat/meris/documentation/meris_3rd_reproc/MERIS_3rd_Reprocessing_Changes.pdf, 2011.

[7] OBPG, NASA, "Ocean Colour Data Reprocessing http://oceancolor.gsfc.nasa.gov/WIKI/OCReproc.html, 2012

[8] B. Nechad, K. Ruddick and G. Neukermans, "Calibration and validation of a generic multi-sensor algorithm for mapping of turbidity in coastal waters.," in *Proc. SPIE Vol. 7473, 74730H.*, 2009.

[9] S. Ouillon, P. Douillet, A. Petrenko, J. Neveux, C. Dupouy, J.-M. Froidefond, S. Andréfouët and A. Muñoz-Caravaca, "Optical Algorithms at Satellite Wavelengths for Total Suspended Matter in Tropical Coastal Waters," *Sensors*, no. 8(7), pp. 4165-4185, 2008.

[10] G. Neukermans, Optical in situ and geostationary satellite-borne observations of suspended particles in coastal waters, Ph.D. dissertation. Université du Littoral - Côte d'Opale, Wimereux, France. p. 210. ed., 2012.

[11] M. Devlin, J. Barry, D. Mills, R. Gowen, J. Foden and D. Sivyer, "Relationships between suspended particulate material, light attenuation and Secchi," *Estuarine, Coastal and Shelf Science*, vol. 79, p. 429–439, 2008.

[12] B. Nechad, K. G. Ruddick and Y.-J. Park, "Calibration and validation of a generic multi-sensor algorithm for mapping of total suspended matter in turbid waters.," *Remote Sensing of Environment*, vol. 114, p. 854–866, 2010.

[13] Z. Lee, A. Weidemann, J. Kindle, R. Arnone, K. R. Carder and D. Curtiss, "Euphotic zone depth: Its derivation and implication to ocean-color remote sensing," *Journal of Geophysical Research: Oceans (1978–2012)*, vol. 112, no. C3, 2007.

[14] Z. Lee, K. L. Carder and R. Arnone, "Deriving inherent optical properties from water color: a multiband quasi-analytical algorithm for optically deep waters.," *Optics Express*, vol. 41, no. 27, pp. 5755-5772, 2002.

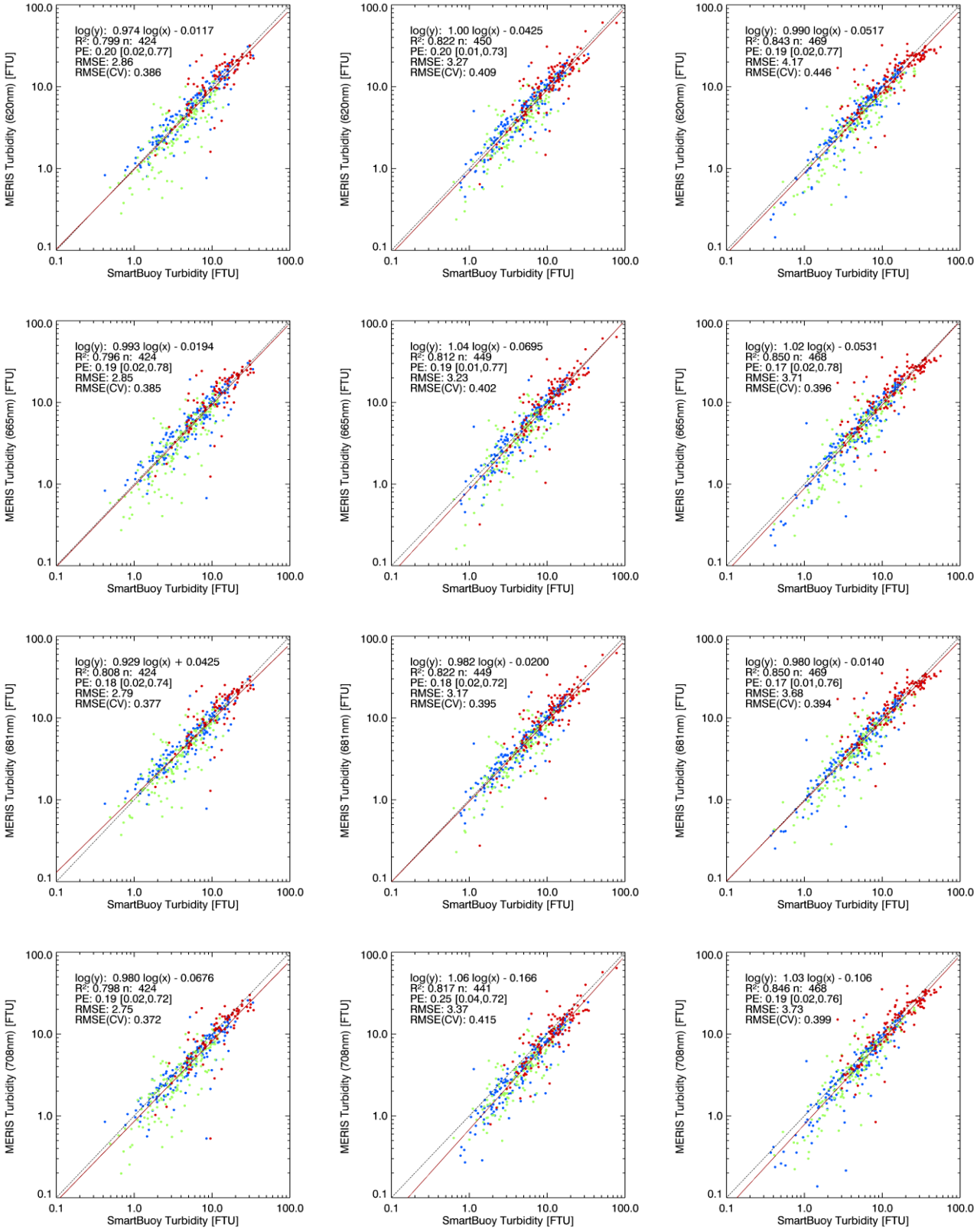

Figure 2 The T-Nechad algorithm as function of SmartBuoy turbidity for M7 (left column), M8 (middle column) and SD (right column), for the 620, 665, 681, and 708nm bands (top to bottom rows). Dots are coloured according to buoy: red: WARP, blue: WGAB, and green: LIVB.

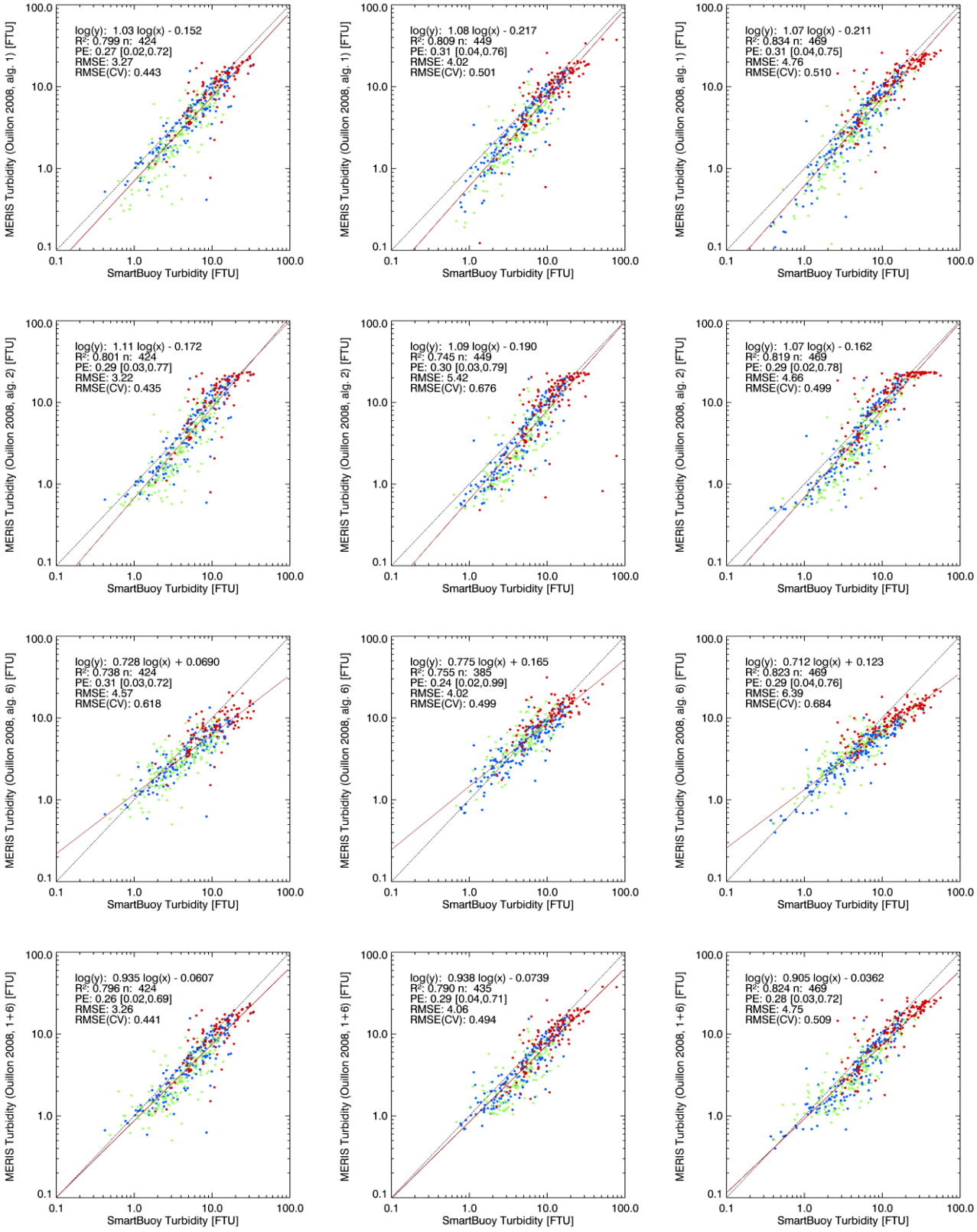

Figure 3 The T-Ouillon algorithm as function of SmartBuoy turbidity for M7 (left column), M8 (middle column) and SD (right column). The first three rows are the turbid polynomial, turbid power law and clear algorithms (respectively algorithms 1, 2, and 6 in **[9]**) The bottom row is the 1+6 merged algorithm. Dots are coloured according to buoy: red: WARP, blue: WGAB, and green: LIVB.

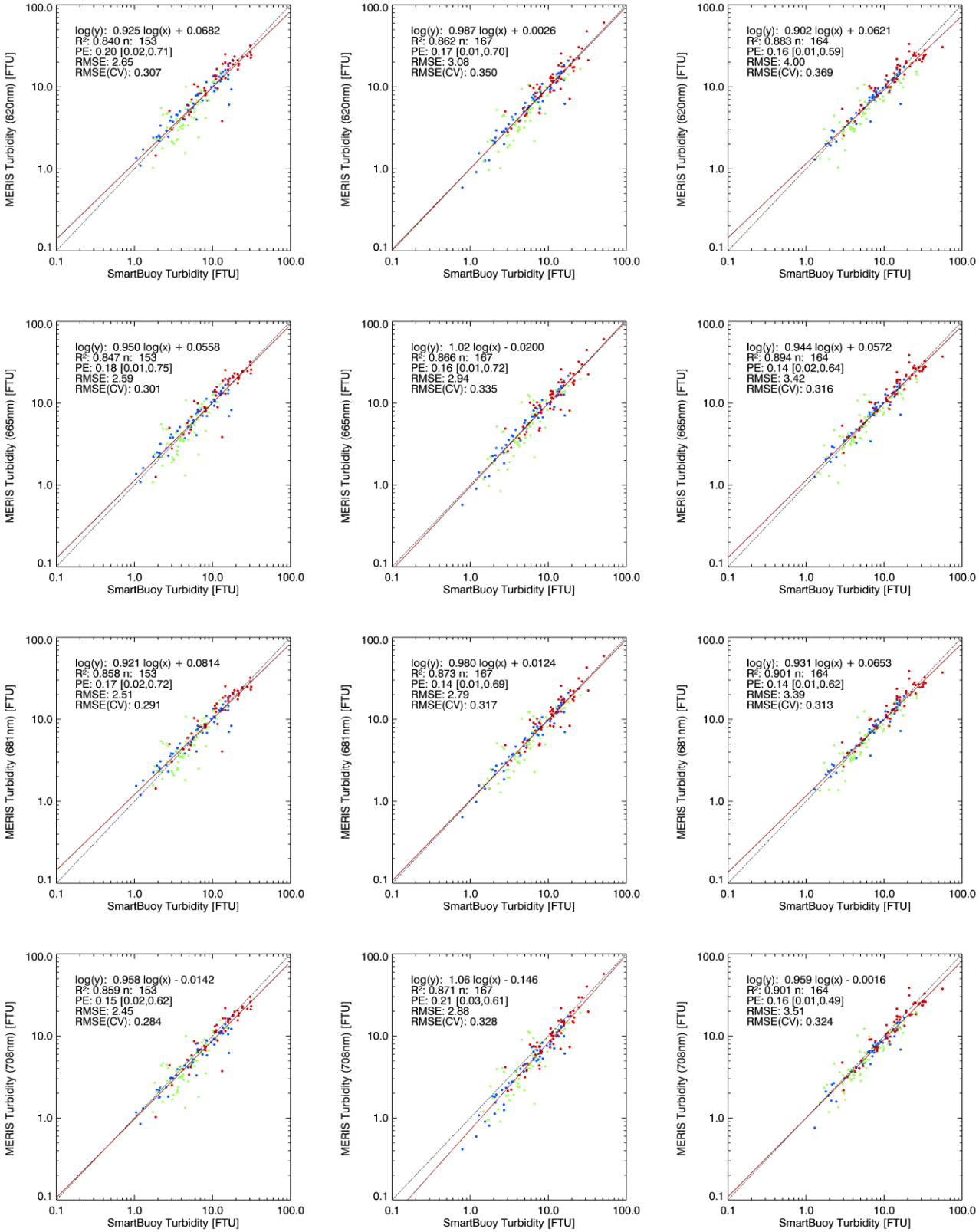

Figure 4 The T-Nechad algorithm with additional quality checks (see text) as function of SmartBuoy turbidity for M7 (left column), M8 (middle column) and SD (right column), for the 620, 665, 681, and 708nm bands (top to bottom rows). Dots are coloured according to buoy: red: WARP, blue: WGAB, and green: LIVB.

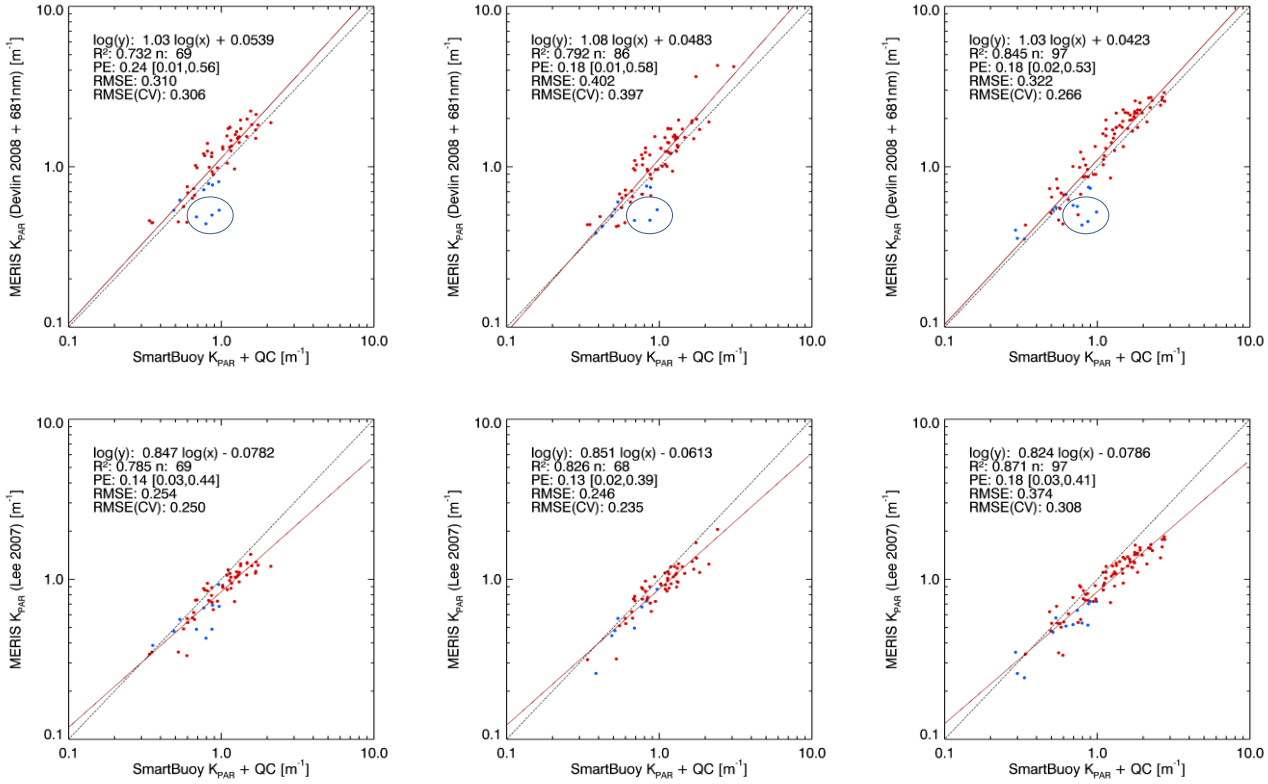

Figure 5 The K_{PAR}-Devlin (top row) and K_{PAR}-Lee (bottom row) algorithms as function of SmartBuoy K_{PAR} for M7 (left column), M8 (middle column) and SD (right column). Dots are coloured according to buoy: red: WARP, and blue: WGAB. The circles indicate points with high in situ fluorescence (see text).